EMBO Molecular Medicine

Genetic disruption of *Pten* in a novel mouse model of tomaculous neuropathy

Sandra Goebbels[1*,†], *Jan H. Oltrogge*[1†], *Susanne Wolfer*[1], *Georg L. Wieser*[1], *Tobias Nientiedt*[1], *Alexander Pieper*[1], *Torben Ruhwedel*[1], *Matthias Groszer*[2], *Michael W. Sereda*[1,3], *Klaus-Armin Nave*[1**]

Keywords: myelin outfolding; neuropathy; rapamycin; Schwann cells; tomacula

DOI 10.1002/emmm.201200227

Received August 05, 2011
Revised February 16, 2012
Accepted February 17, 2012

'Tomacula' and myelin outfoldings are striking neuropathological features of a diverse group of inherited demyelinating neuropathies. Whereas the underlying genetic defects are well known, the molecular mechanisms of tomacula formation have remained obscure. We hypothesized that they are caused by uncontrolled, excessive myelin membrane growth, a process, which is regulated in normal development by neuregulin-1/ErbB2, PI3 Kinase signalling and ERK/MAPK signalling. Here, we demonstrate by targeted disruption of *Pten* in Schwann cells that hyperactivation of the endogenous PI3 Kinase pathway causes focal hypermyelination, myelin outfoldings and tomacula, even when induced in adult animals by tamoxifen, and is associated with progressive peripheral neuropathy. Activated AKT kinase is associated with PtdIns(3,4,5)P_3 at paranodal loops and Schmidt–Lanterman incisures. This striking myelin pathology, with features of human CMT type 4B1 and HNPP, is dependent on AKT/mTOR signalling, as evidenced by a significant amelioration of the pathology in mice treated with rapamycin. We suggest that regions of non-compact myelin are under lifelong protection by PTEN against abnormal membrane outgrowth, and that dysregulated phosphoinositide levels play a critical role in the pathology of tomaculous neuropathies.

INTRODUCTION

Inherited neuropathies, known as Charcot Marie Tooth disease (CMT) or hereditary motor and sensory neuropathies (HMSN), comprise a genetically heterogeneous group of neuromuscular disorders of considerable prevalence (Skre, 1974). The main clinical features of CMT diseases are a distally accentuated muscle weakness and atrophy, foot deformities and sensory deficits. While progressive loss of long axons is a common feature, in the demyelinating forms, there is also a characteristic slowing of nerve conduction velocity (NCV) associated with primary abnormalities of the myelin architecture (Berger et al, 2006). Within the last 20 years, numerous CMT disease genes have been identified and specific animal models have been generated (Meyer Zu Hörste & Nave, 2006; Pareyson et al, 2009; Scherer & Wrabetz, 2008). Nonetheless, the molecular mechanisms that link different primary genetic defects with the final common pathway in CMT neuropathies are poorly understood.

Several reports have identified CMT-relevant mutations in genes encoding proteins with phosphoinositide binding domains like *dynamin 2* (Zuchner et al, 2005) and *FGD4/frabin* (Delague et al, 2007; Stendel et al, 2007) and in phosphoinositide phosphatases such as the D5-phosphatase FIG4 (in CMT-4J) that dephosphorylates PtdIns(3,5)P2 (Chow et al, 2007). Mutations in the gene for the myotubularin-related protein-2 (MTMR2), a D3-phosphatase that dephosphorylates both PtdIns(3)P and PtdIns(3,5)P2, underlie the autosomal recessive form CMT-4B1 (Bolino et al, 2000; Bolis et al, 2005; Bonneick et al, 2005; Houlden et al, 2001; Nelis et al, 2002). A similar neuropathy, CMT-4B2, is caused by mutations in the gene for MTMR13/Set-binding factor-2 (SBF2). While this protein is catalytically inactive, it forms a tetrameric complex with MTMR2, thereby strongly increasing that enzyme's activity

(1) Max-Planck-Institute of Experimental Medicine, Göttingen, Germany
(2) Institut du Fer-à-Moulin, Inserm, University Pierre and Marie Curie, Paris, France
(3) Department of Clinical Neurophysiology, University of Göttingen, Göttingen, Germany
***Corresponding author:** Tel: +49 551 3899 747; Fax: +49 551 3899 758; E-mail: sgoebbels@em.mpg.de
****Corresponding author:** Tel: +49 551 3899 754; Fax: +49 551 3899 758; E-mail: nave@em.mpg.de
[†]These authors contributed equally to this work

(Berger et al, 2006; Bolis et al, 2007; Robinson et al, 2008; Tersar et al, 2007). Mechanistically, it is still incompletely understood why the dysregulation of phosphoinositides, such as PtdIns(3,5)P2, in Schwann cells perturbs myelination and myelin sheath maintenance (Suter, 2007).

At the same time it has become clear that a diverse group of inherited demyelinating neuropathies is associated with extensive myelin production that manifests histologically as myelin outfoldings or focal thickening of the myelin sheath ('tomacula'). This ranges from CMT-4B (see above), CMT-4H (mutations in the *FGD4/frabin* gene; Delague et al, 2007; Fabrizi et al, 2009; Stendel et al, 2007), CMT-4F (mutations in the *periaxin* gene) (Gillespie et al, 2000; Takashima et al, 2002), and CMT-1B (specific mutations in the myelin protein zero gene, *MPZ*; Fabrizi et al, 2000) to hereditary neuropathy with liability to pressure palsies (HNPP, haplo-insufficiency of *PMP22*; Adlkofer et al, 1997).

We hypothesized that one candidate responsible for abnormal myelin overproduction is phosphatidylinositol-3,4,5-trisphosphate (PtdIns(3,4,5)P3). This signalling lipid is generated from the pool of available PtdIns(4,5)P2 by the activity of phosphoinositide-3-kinase (PI3K). In myelinated nerves, PI3K is activated when axonal NRG1 type III binds to glial ErbB2/ErbB3 receptor heterodimers and PtdIns(3,4,5)P3 promotes myelination in an AKT/PKB-dependent fashion, at least *in vitro* (Liang et al, 2007; Maurel & Salzer, 2000; Ogata et al, 2004; Taveggia et al, 2005). PI3K activity is antagonized by the lipid phosphatase PTEN (*phosphatase and tensin homolog*) (Stiles et al, 2004; Suzuki et al, 2008). PTEN inhibits myelination (Goebbels et al, 2010), specifically in conjunction with the mammalian Disc-large homolog Dlg1 in Schwann cells (Cotter et al, 2010).

In the present study, we characterized a novel neuropathy model in mice and tested the hypothesis that myelin outfoldings and tomacula result from a local loss of myelin growth control, modelled by abnormal PtdIns(3,4,5)P3 stimulation in Schwann cells. This was achieved by analysing a cell-specific mouse mutant of PTEN. We show that the elevation of PI(3,4,5)P3 levels in mutant Schwann cells is sufficient to cause myelin outfoldings and tomacula. This pathology is prominent even when the *Pten* expression is targeted in adult animals, *i.e.* after the completion of myelination. We suggest that PTEN in myelinating Schwann cells serves to protect the mature sheath from aberrant membrane outgrowth at paranodal loop regions and Schmidt–Lanterman incisures, which emerge as myelin growth zones. Amelioration of the neuropathology by the treatment of mice with rapamycin demonstrates an essential role of the mTOR downstream signalling in tomacula formation, which is of possible relevance for the development of novel therapies.

RESULTS

Focal hypermyelination in the PNS of mice lacking PTEN in Schwann cells

We have previously generated mice that lack expression of a floxed *Pten* gene in oligodendrocytes and Schwann cells, following expression of *Cre* under control of the *Cnp1* gene regulatory region (Goebbels et al, 2010). In peripheral nerves, this recombination led to significantly increased levels of PtdIns(3,4,5)P3 and decreased levels of PtdIns(4,5)P2, associated with significant hypermyelination (as evidenced by decreased g-ratios) of sciatic nerve axons smaller than 2 μm in diameter (Goebbels et al, 2010). These findings support the role of PI3K signalling in myelination control.

Western blot analysis of sciatic nerve lysates from conditional *Pten* mutants confirmed the significant downregulation of PTEN protein and an enhanced phosphorylation of the known PI3K downstream target proteins AKT, mTOR and S6, but no changes in the level of phosphorylated ERK1/2 (Fig 1A). When we determined the degree of myelination for axons larger than 2 μm in diameter, we found a g-ratio for the *Pten* mutants ($Pten^{flox/flox*}Cnp^{Cre/+}$) of 0.6345 (±0.0094), which is not significantly different from controls ($Pten^{flox/flox*}Cnp^{+/+}$; 0.6339 ± 0.0129) (Fig 1B). Surprisingly, we noticed that numerous axons exhibited instead a hypermyelination of focal origin, *i.e.* tomacula and myelin outfoldings (left panels in Fig 1C). This finding is specific for the conditional *Pten* null mutants and not present in heterozygous $Pten^{flox/+*}Cnp^{Cre/+}$ mice (right panels in Fig 1C), implying that the complete loss of PTEN expression is required to develop focal myelin pathology. We quantified the onset and progression of the myelin abnormalities (Fig 2A) by analysing *Pten* mutants and controls at postnatal day (P) 12 and at 3 months of age (P90) ($n = 3$ for each genotype and age) by comparing methylene blue-stained semithin cross sections of sciatic nerves. Already at P12, abnormal Schwann cell-axon units could be observed with 1.4% of the fibres affected by tomaculous pathology and 0.2% exhibiting 'comma-shaped' myelin outfoldings. At P90, 6.6% of mutant fibres showed a tomaculous pathology and 2.8% exhibited comma-shaped myelin outfoldings. Given the frequency of tomacula in cross-sections of the sciatic nerve, we must assume that virtually all large calibre axons are affected somewhere along their length by focal myelin overgrowth.

By electron microscopy (EM), myelin outfoldings in cross sections contained no axonal structures (arrowhead in Fig 2C). Myelin membranes were either facing away from the axon cylinder or coiled around the axon presumably representing an initial stage in the formation of a tomaculum (Fig 2B and C). In more advanced forms, the excess myelin lamellae that were folded around the axons appeared fused to the original myelin sheath (tomaculum; Fig 2D and G). With age, complexity of the neuropathology progressed. While some outfoldings were orientated perpendicular to the nerve axis (termed 'comma-shaped' outfoldings, Fig 2B and C), others were aligned parallel to the axon. The latter appeared (in cross sections) as concentric rings of myelin, adjacent to a 'normally' myelinated axon (termed 'recurrent loops'; Fig 2E). 'Evaginating' and also 'invaginating' recurrent loops (Fig 2E and F) always showed the same number of myelin lamellae, periodicity and degree of compaction as the myelin sheath from which they had originated. EM images of redundant myelin also revealed axons that were displaced, deformed or constricted (Fig 2D, F and G).

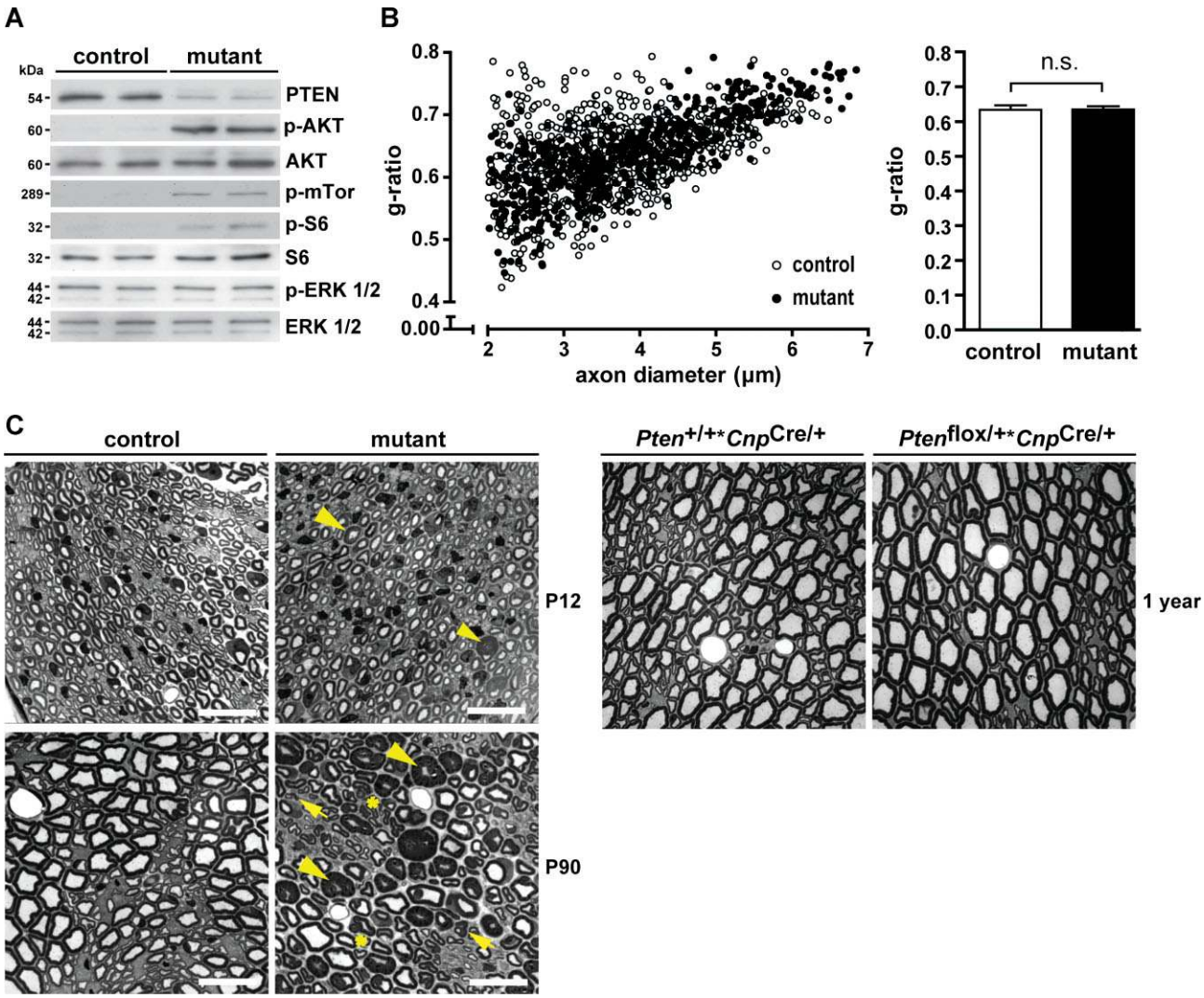

Figure 1. Focal hypermyelination in PTEN mutants.

A. Westernblot analysis of sciatic nerve lysates obtained from two controls and two mutants at the age of 3 months. PTEN protein is decreased in the mutants and P-AKT, P-mTOR and P-S6 levels are increased. In contrast the levels of phosphorylated ERK1 and ERK2 are unchanged in mutants compared to controls.

B. Scatter plot depicting g-ratios (ordinate) of 1.5 month-old mutant and age-matched control mice in relation to the axon diameter (abscissa) based on semithin sections of sciatic nerves at comparable levels (left panel). Axons with calibres larger than 2 μm in diameter show no alteration in myelin sheath thickness in mutants when compared to controls (right panel) ($n = 6$ for mutants; $n = 8$ for controls; $p = 0.9728$). Error bars represent the SEM. The p value was calculated by two-tailed Student's t-test.

C. Left panels: light-microscopic analysis of myelin abnormalities on sciatic nerve transverse semithin-sections (500 nm) of mutants ($Pten^{flox/flox*}Cnp^{Cre/+}$) and controls ($Pten^{flox/flox*}Cnp^{+/+}$) at the indicated ages. Mutant nerves are characterized by a progressive development of myelin abnormalities like tomacula (arrowheads), comma-shaped myelin outfoldings (arrows) and recurrent myelin loops (asterisks). Scale bars, 20 μm. Right panels: light-microscopic analysis of sciatic nerve semithin cross-sections (500 nm) reveals no myelin pathology in heterozygous $Pten^{flox/+*}Cnp^{Cre/+}$ mice when compared to $Pten^{+/+*}Cnp^{Cre/+}$ controls at 1 year of age.

Hence, we observed signs of axonal damage, which included macrophage processes removing redundant myelin (Fig 2H). As signs of perturbed axonal transport leading to axonal degeneration we observed the accumulation of organelles (mainly mitochondria) in the axoplasm (Fig 2I). More progressed forms were characterized by irregular distribution of neurofilaments and microtubules (Fig 2J) and Wallerian-type axonal degeneration with myelin debris (Fig 2K).

Myelin abnormalities emanating from non-compacted regions

Teased fibre preparations (osmicated, age P46) and electron microscopic analysis of longitudinal sciatic nerve sections (P30) revealed that myelin abnormalities predominantly originated from paranodal regions and Schmidt–Lanterman incisures (Fig 3A and B). These regions of non-compacted myelin are thought to represent zones in which controlled membrane

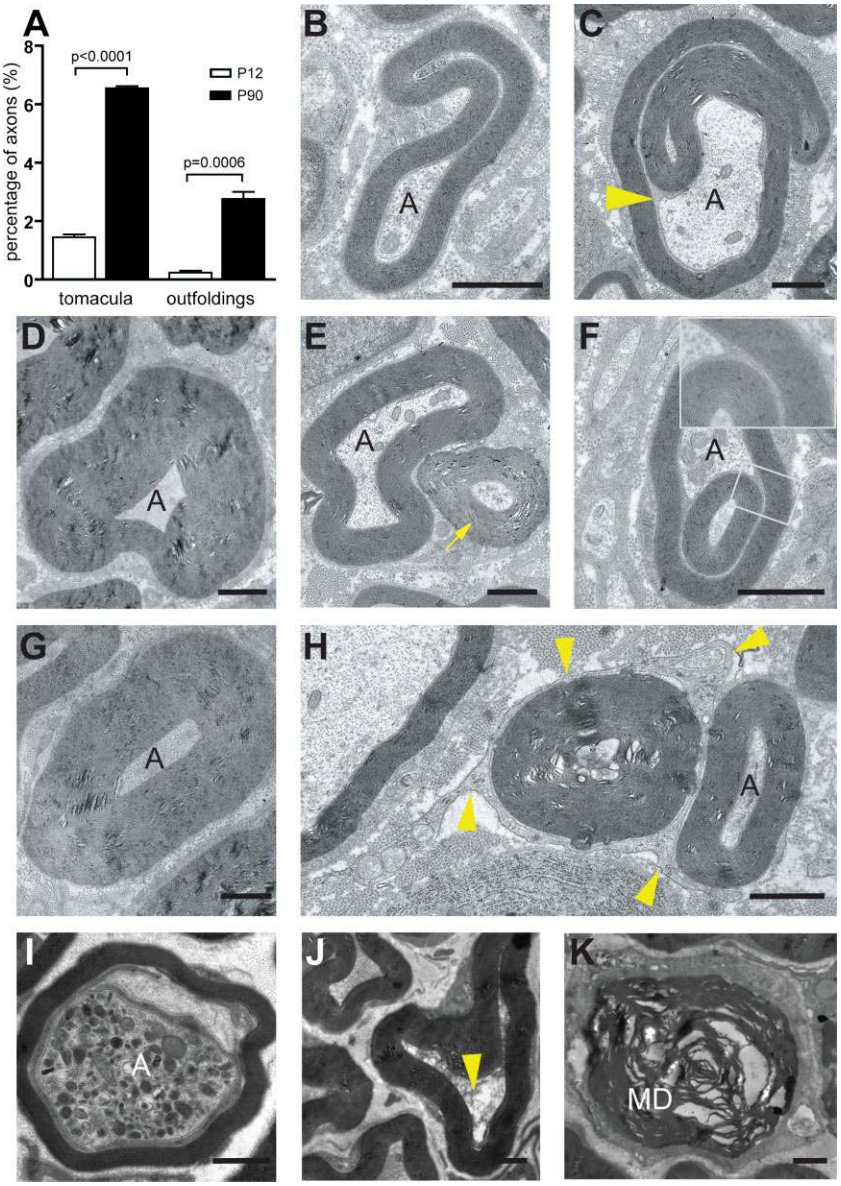

Figure 2. Quantitative and ultrastructural analysis of abnormal axon/Schwann cell units.

A. When counted on semithin sciatic nerve cross sections, tomacula and comma-shaped outfoldings increased in number with age (tomacula: $1.44 \pm 0.10\%$ for P12 mutants and $6.55 \pm 0.07\%$ for P90 mutants; outfoldings: $0.24 \pm 0.07\%$ for P12 mutants and $2.76 \pm 0.25\%$ for P90 mutants; $n = 3$ per genotype and age). Error bars represent the SEM. *p* values were calculated by two-tailed Student's *t*-test.

B–K. Ultrastructural analysis of focally redundant myelin in mutant sciatic nerves appearing as comma-shaped outfoldings (**B, C**), tomacula (**D**) and recurrent loops (arrow in **E**). Myelin outfoldings contain no axonal structures (arrowhead in **C**). Invaginating recurrent loops exhibit the same spacing and number of lamellae as the myelin sheath they originate from (inset in **F**). Nearly regular appearing hypermyelination also occurs (**G**). Occasionally, processes of macrophages are observed that actively remove redundant myelin (arrowheads in **H**). Accumulation of axoplasmic organelles (**I**), degeneration of microtubules and neurofilaments (arrowhead in **J**), and Wallerian-type degeneration (**K**) indicate disturbed axonal functions. A, axon. MD, myelin debris. Scale bars, 1 μm.

incorporation and myelin growth takes place. We therefore asked whether the lack of PTEN would mimic abnormally enhanced axon–glia signalling and PI3K activation in these regions. Indeed, when p-AKT was used as an indirect sensor of elevated PtdIns(3,4,5)P3 levels, and sections were co-immunostained for P0 (MPZ, a marker of compact myelin) and myelin-associated glycoprotein (MAG, a marker of non-compacted myelin), we found a striking localization of p-AKT in MAG-positive Schmidt–Lanterman incisures and paranodes (Fig 4A and B). This suggests that incisures and paranodes are regions in which PTEN normally downregulates the level of PtdIns(3,4,5)P3 and that this signalling lipid, if experimentally enhanced in our conditional mutants, drives a local deposition of myelin membranes. The cell polarity proteins Par-3 and Dlg1, which interact with PTEN via their PDZ domains (Adey et al, 2000; Feng et al, 2008), have been localized in regions of non-compact myelin (Bolino et al, 2004; Poliak et al, 2002) and have independently been associated with a role in myelination (Bolis et al, 2009; Chan et al, 2006; Cotter et al, 2010). The localization of both proteins was unchanged in *Pten* mutant nerves when immunohistochemically stained in teased fibre preparations (Fig 4C).

Reduced nerve conduction velocity and compound muscle action potentials

To determine whether *Pten* conditional mutants model a human peripheral neuropathy by clinical criteria, electrophysiology of the sciatic nerve was performed on mice at age P43, *i.e.* when clear histological signs of pathology are present. Motor NCV was slower in *Pten* mutants (17.7 ± 3.7 m/s) compared to age-matched controls (26.7 ± 3.8 m/s). In addition we observed markedly reduced compound muscle action potentials (CMAP)

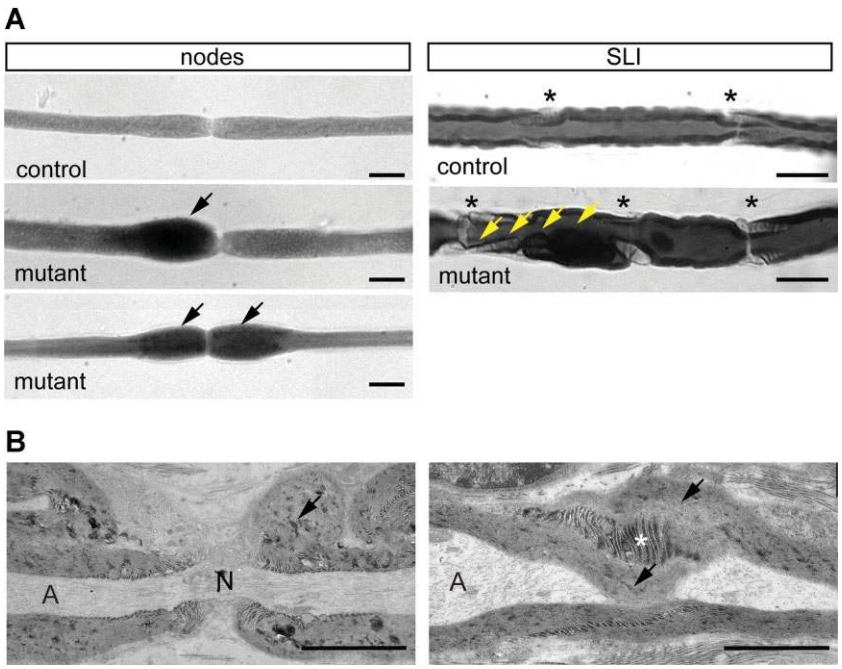

Figure 3. Myelin abnormalities preferentially originate at regions of non-compact myelin.

A. Osmicated teased nerve fibres from 1.5 month-old control and mutant mice. Focal myelin thickenings preferentially originate at paranodal regions (black arrows) and Schmidt–Lanterman incisures (SLI) (yellow arrows). SLI are indicated by asterisks. Note in left panel that either one or both paranodal regions can be affected. Scale bars, 10 μm.

B. Ultrastructural appearance of exuberant myelin growth (arrows) at paranodal regions (left panel) and SLI (marked by asterisk in right panel). A, axon; N, node. Scale bars, 2 μm.

when recorded after distal (7.4 ± 2.7 mV in mutants *vs.* 21.8 ± 2.2 mV in controls) and proximal stimulation (5.3 ± 2.4 mV *vs.* 19.8 ± 2.7 mV) (Fig 5 and Table 1).

Rapamycin treatment ameliorates myelin abnormalities

Ablation of *Pten* is generally associated with the constitutive activation of PI3K downstream effectors, including the serin-threonine kinases AKT and mTOR. To analyse whether inhibition of mTOR signalling in turn interferes with focal hypermyelination we treated *Pten* mutants and littermate controls with rapamycin, a specific mTOR inhibitor. The drug was given from P13, when mutant sciatic nerves exhibited only minor myelin pathology, to age P43, when the clinical phenotype was more pronounced. Both rapamycin-treated mutants and controls gained less weight in this time window than the placebo-treated animals (weight gain of controls, 6.8 ± 0.6 g with rapamycin, $n = 7$ *vs.* 9.4 ± 0.8 g without rapamycin, $n = 7$, $p < 0.05$; weight gain of mutants, 7.1 ± 0.2 g with rapamycin, $n = 7$ *vs.* 11.2 ± 0.3 g without rapamycin, $n = 6$, $p < 0.001$). This was expected and is consistent with the known role of mTOR in growth control.

To evaluate specificity and efficiency of rapamycin-mediated inhibition of mTOR signalling, we analysed the activity of upstream and downstream kinases of the mTOR pathway in *Pten* mutants. Because mTOR signalling activates S6 Kinase, which phosphorylates ribosomal S6 (Saitoh et al, 2002), we determined the level of phospho-S6 (p-S6) as an indicator of mTOR activity. By Westernblot analyses of sciatic nerve lysates rapamycin-treated mutants had strongly diminished p-S6 levels compared to placebo-treated mutants, demonstrating efficient blockage of the mTOR pathway (Fig 6A). In contrast, levels of pAKT were elevated in sciatic nerves of both placebo- and rapamycin-treated mutants (Fig 6A). This confirms that rapamycin blocked mTOR signalling without influencing the upstream protein kinase AKT.

The loss of *Pten* from Schwann cells recruits more axons for myelination (Goebbels et al, 2010). Accordingly, when quantified at P43, placebo-treated *Pten* mutant sciatic nerves harboured significantly more myelinated axons than control nerves (4289 ± 90.99 in mutants *vs.* 3684 ± 159.8 in controls). Since this increase in the number of myelinated axons was not lowered by the administration of rapamycin (4240 ± 116.5 in treated mutants *vs.* 3721 ± 103.2 in treated controls; Fig 6B) we conclude that at the onset of treatment the number of myelin profiles in the mutants is already set.

Myelinated axons were found more loosely spaced in (placebo-treated) *Pten* mutants than in wildtype controls (2.512 ± 0.16 axons/100 μm^2 in mutants *vs.* 4.044 ± 0.183 axons/100 μm^2 in controls). Consequently, in rapamycin-treated mutants myelinated axons were more densely packed than those in placebo-treated mutants (3.465 ± 0.111 axons/100 μm^2 in treated mutants; Fig 6C). In wildtype controls rapamycin had no obvious effect on the density of myelinated axons.

To assess the effect of rapamycin on myelin pathology we quantified tomacula, comma-like outfoldings, and evaginating recurrent loops in sciatic nerve cross sections of rapamycin and placebo-treated mutants and their respective wildtype controls (hereafter referred to as mutants$^{(+Rap)}$, mutants$^{(-Rap)}$, controls$^{(+Rap)}$ and controls$^{(-Rap)}$, respectively). As expected, the number of myelin abnormalities was significantly higher in mutants$^{(-Rap)}$ than in controls$^{(-Rap)}$ (Fig 6D–F). After 30 days of treatment, tomacula were reduced by 74% in mutants$^{(+Rap)}$ (52 ± 12.87 per cross section) compared to mutants$^{(-Rap)}$ (209 ± 20.76) (Fig 6D). Similarly, recurrent loops were reduced by 75% (17.88 ± 3.393 in mutants$^{(+Rap)}$ *vs.* 72.17 ± 7.897

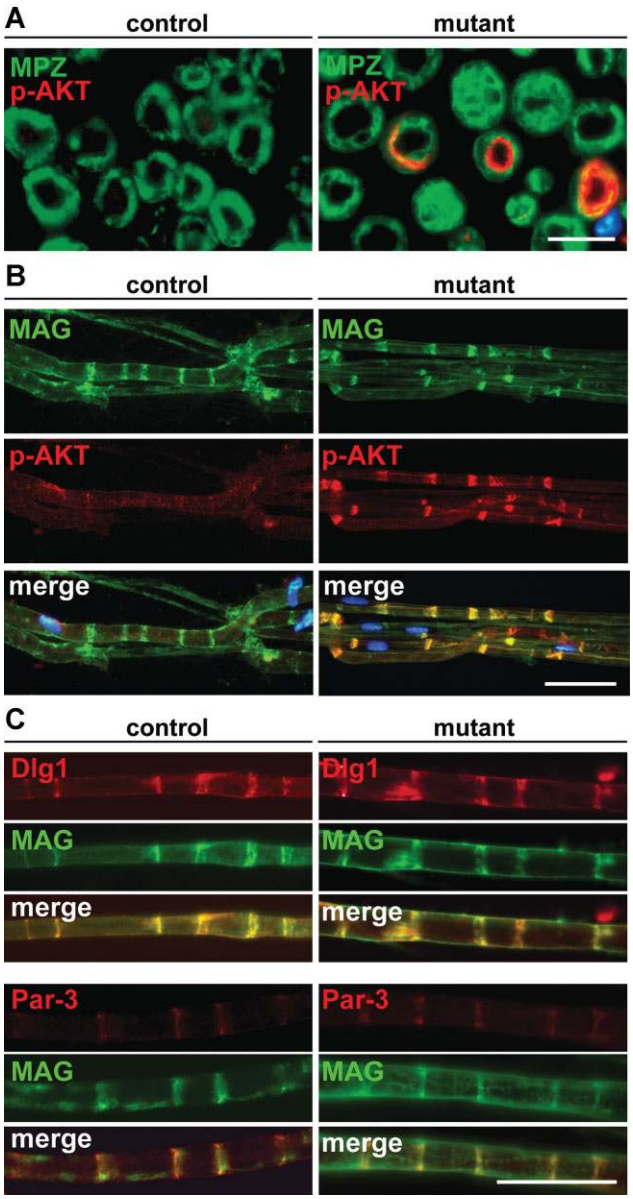

Figure 4. Enhanced AKT activity and unaltered expression levels of Dlg1 and Par-3.

A. Immunostaining of sciatic nerve cross sections with antibodies against p-AKT (in red) and MPZ as a marker of compact myelin (in green). Scalebar, 10 μm.

B. Teased sciatic nerve fibres stained with antibodies against p-AKT (in red) and MAG as a marker of non-compact myelin (in green). Scale bars, 50 μm.

C. Costaining of MAG and Dlg1 (upper panels) and MAG and Par-3 (lower panels). Dlg1 and Par-3 are similarly enriched in mutants and controls in regions of non-compact myelin. Scale bar, 50 μm.

mutants$^{(-Rap)}$; Fig 6E). Finally, also comma-like outfoldings were reduced by 49% (60.13 ± 13.37 in mutants$^{(+Rap)}$ *vs.* 117.2 ± 6.882 in mutants$^{(-Rap)}$; Fig 6F). Rapamycin treatment did not change the myelin profile in control mice. Taken together, these results demonstrate that enhanced mTOR downstream signalling contributes to the myelin pathology of *Pten* mutant mice.

Focal hypermyelination after inactivation of Pten in Schwann cells of adult mice

To determine whether changes in phosphoinositide metabolism would also cause neuropathy with focally folded myelin after development has completed, we inactivated the floxed *Pten* gene in adult mice by tamoxifen (TM) induced Cre recombination. We intercrossed *Pten*$^{flox/flox}$ mice to a TM inducible *Plp*-CreERT2 driver line (Leone et al, 2003). Two month-old double transgenics (*Pten*$^{flox/flox}$**Plp*-CreERT2) and *Pten*$^{flox/flox}$ controls received intraperitoneal TM injections for 10 consecutive days, and were analysed histologically 3.5 months later. Indeed, all previously documented myelin abnormalities, including comma-shaped outfoldings, recurrent loops and tomacula were also found in these double transgenic mice (Fig 7A and B), albeit to a lesser extent. This demonstrates that PtdIns(3,4,5)P3 levels must be regulated by PTEN also in adult Schwann cells in order to maintain the integrity of the mature myelin sheath.

DISCUSSION

We have shown that the ablation of the lipid phosphatase gene *Pten* in Schwann cells leads to a progressive peripheral neuropathy in mice that resembles features of certain human forms of CMT diseases, such as CMT4B1 and HNPP, which are genetically unrelated. In this novel disease model, the focal forms of exuberant myelin growth were documented at the EM level as myelin outfoldings, recurrent loops and tomacula. At the physiological level, they are associated with a diffuse slowing of conduction velocity. Although the number of myelinated axons was not diminished, CMAP amlitudes were reduced after both proximal and distal stimulation suggesting failures in axonal conduction. However, we do not consider *PTEN* an inherited neuropathy disease gene. In mice, *Pten* null

Table 1. Reduced NCV and CMAP amplitudes in *Pten* mutant mice

	Controls	Mutants
CMAP amplitudes (mV)		
Proximal stimulation	19.8 (±2.7)	5.3 (±2.4)[a]
Distal stimulation	21.8 (±2.2)	7.4 (±2.7)[b]
Motor NCV (m/s)	26.7 (±3.8)	17.7 (±3.7)[c]
Motor latency (ms)		
Proximal stimulation	2.1 (±0.1)	2.4 (±0.2)
Distal stimulation	1.3 (±0.1)	1.4 (±0.1)
F-wave latency (ms)		
Proximal stimulation	4.7 (±1.1)	6.2 (±0.8)
Distal stimulation	6.2 (±0.5)	7.1 (±0.7)

Electrophysiological recordings are from P43 old mutant (*Pten*$^{flox/flox}$**Cnp*$^{Cre/+}$) and age matched control (*Pten*$^{flox/flox}$**Cnp*$^{+/+}$) mice. All data are expressed as mean ± SEM. Sample size is $n = 3$ per genotype. Differences between controls and mutants are significant where indicated.

[a] $p = 0.0021$.

[b] $p = 0.0022$.

[c] $p = 0.0422$.

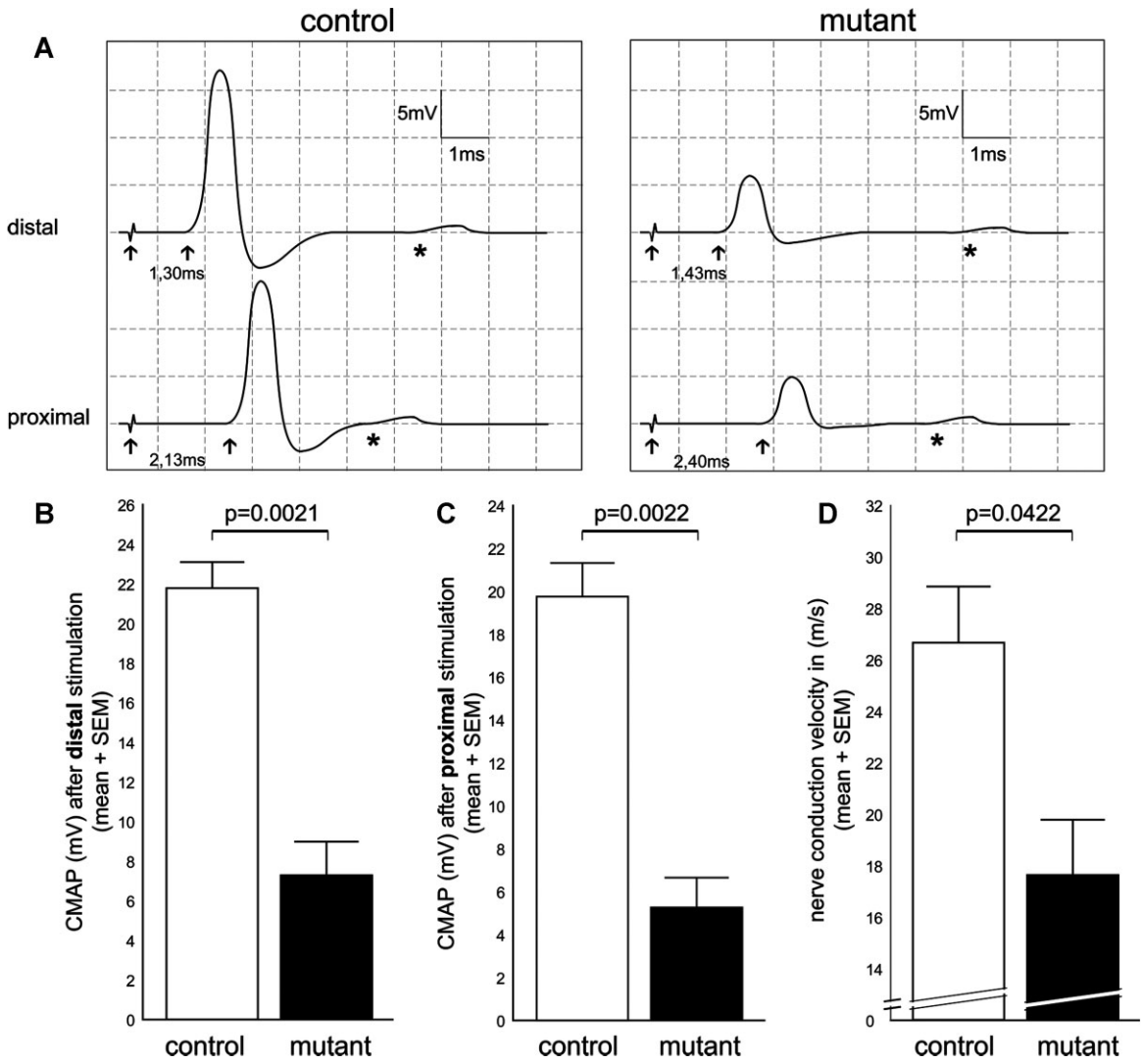

Figure 5. Reduced NCV and CMAP.

A. Representative traces of sciatic nerve CMAPs recorded from a foot muscle after proximal and distal stimulation. Arrows indicate the stimulus and the onset of the CMAP. Asterisk marks the F-wave latency. Compared to controls, Pten mutants display prolonged latencies and decreased CMAP amplitudes.

B–D. Motor nerve conduction studies of 43 days old controls and mutants ($n = 3$ per group). Mutants show significantly reduced CMAP amplitudes after **(B)** distal and **(C)** proximal stimulation. **(D)** Sciatic NCV is significantly slowed in Pten mutants compared to controls. Error bars represent the SEM. *p* values were calculated by two-tailed Student's *t*-test.

mutants are not viable (Di Cristofano et al, 1998), and human (heterozygous) germline mutations cause a rare PTEN autosomal-dominant harmatoma syndrome (Hobert & Eng, 2009) comprising four major clinically distinct syndromes with only anecdotal reports of neuropathy in Cowden disease (Waite & Eng, 2002).

In *Pten*-mutant mice, the focal hypermyelination is a cell autonomous defect of myelinating Schwann cells. *Cnp-Cre* mice (Lappe-Siefke et al, 2003) recombine target genes early in the Schwann cell lineage (Goebbels et al, 2010). While we cannot rule out the occasional deletion of *Pten* in common precursor cells of Schwann cells and DRG neurons (or oligodendrocytes and spinal motor neurons; Genoud et al, 2002), the reported phenotype is unlikely to be caused by abnormal behaviour of a few mutant neurons. Cell autonomy is also supported by a similar phenotype in combination with the *Plp-CreERT2* transgene and tamoxifen treatment of adult mice, which does not lead to recombination in (embryonic) neuron–glia progenitors.

Central nervous system (CNS) axons and small calibre axons in the peripheral nervous system (PNS) are morphologically hypermyelinated in *Pten* mutant mice, as evidenced by decreased g-ratios (Goebbels et al, 2010). However, our mutants differ markedly from mice that overexpress NRG1 type III in neurons and are uniformly hypermyelinated (Michailov et al, 2004) because they exhibit an unusual degree of focal hypermyelination in the PNS. Thus, the absence of PTEN

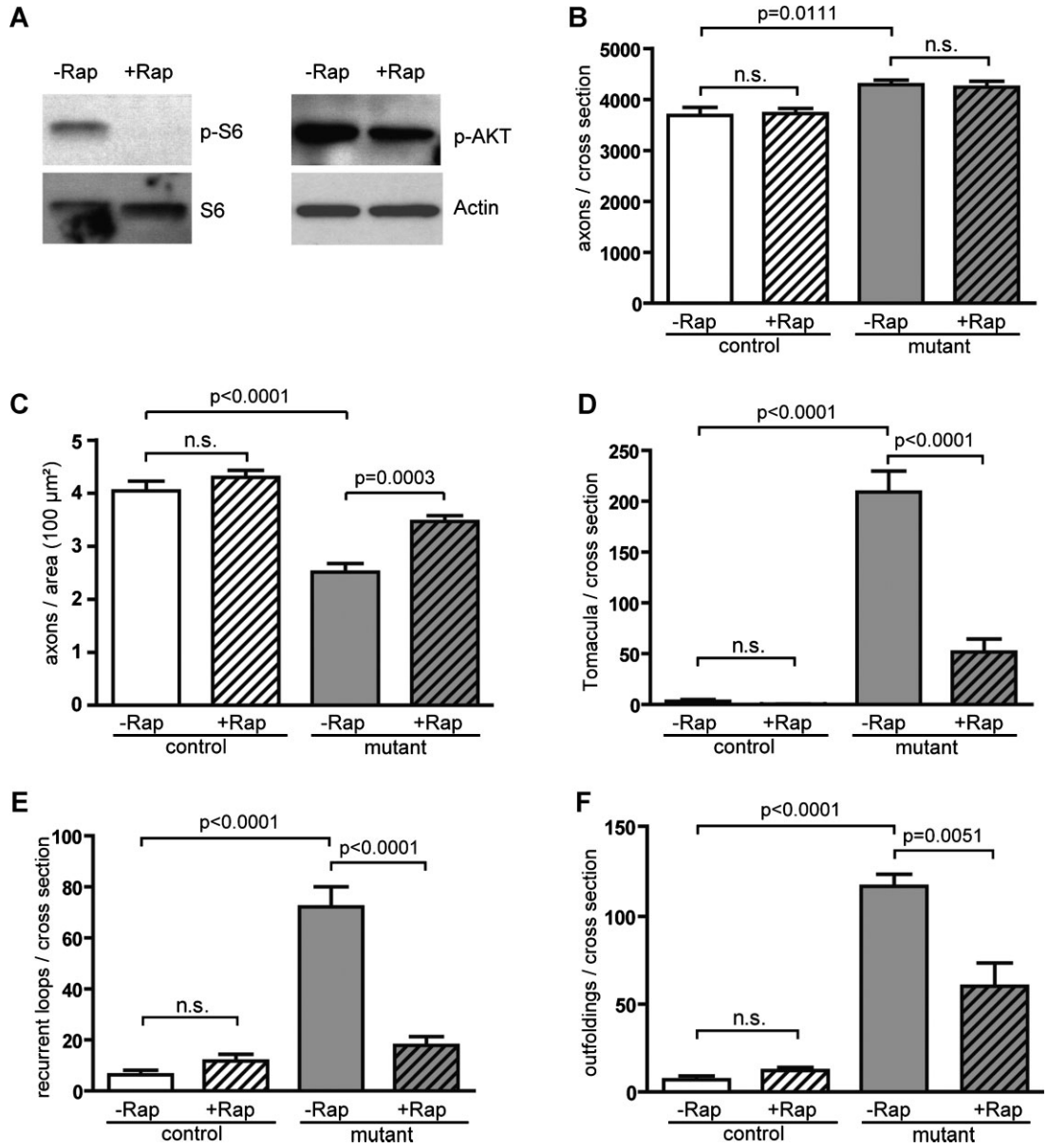

Figure 6. Rapamycin treatment ameliorates myelin pathology in Pten mutants.

A. Westernblots of sciatic nerve lysates from mutant mice treated with placebo (−Rap) or rapamycin (+Rap) from P13 to P43. Rapamycin treatment substantially reduced downstream phosphorylation of S6 but did not lower total protein levels of S6 or levels of P-AKT when compared to Actin as a loading control.

B–F. When quantified on semithin cross sections, the total number of myelinated axons was invariably higher in mutants than in controls and not influenced by rapamycin treatment (**B**). While the density of myelinated axons was reduced in mutants$^{(-Rap)}$ when compared to controls$^{(-Rap)}$, rapamycin treatment significantly restored the axonal density in mutants$^{(+Rap)}$ closer to control levels (**C**). Rapamycin treatment also significantly lowered the number of tomacula (**D**), recurrent loops (**E**) and outfoldings (**F**) in the mutants$^{(+Rap)}$ when compared to mutants$^{(-Rap)}$. Controls$^{(-Rap)}$, $n = 8$; controls$^{(+Rap)}$, $n = 6$; mutants$^{(-Rap)}$, $n = 6$; and mutants$^{(+Rap)}$, $n = 8$. Error bars represent the SEM. *p* values were calculated by two-tailed Student's *t*-test.

(and enhanced PI3K downstream signalling) is not simply a phenocopy of enhanced NRG1/ErbB signalling in Schwann cells (Michailov et al, 2004; Taveggia et al, 2005). This conclusion is in agreement with recent studies revealing a role of ERK1/2 kinase in mediating NRG1/ErbB signalling in Schwann cells (Newbern & Birchmeier, 2010; Newbern et al, 2011). However, the elevated levels of PtdIns(3,4,5)P_3 in *Pten* mutant Schwann cells were clearly associated with a focally hypermyelinating phenotype that was significantly ameliorated by the treatment of mice with rapamycin. The latter suggests that downstream of PI3K/AKT, the rapamycin-sensitive mTOR complex 1 (mTORC1, including mTOR and Raptor) not only promotes

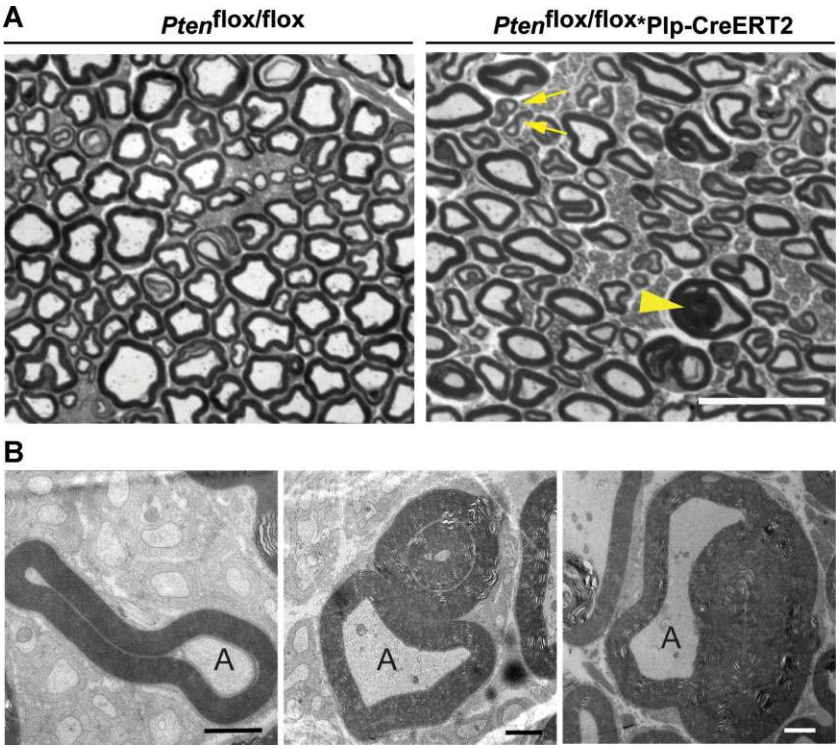

Figure 7. Myelin pathology after inactivation of Pten in adult mice.

A. Semithin sections of a control mouse (*Pten*$^{flox/flox}$) and a double transgenic mutant mouse harbouring a *Plp*-CreERT2 transgene (*Pten*$^{flox/flox*}$*Plp*-CreERT2). Mice were treated with TM at 2 months of age and analysed 3.5 months later. Outfoldings (arrows) and tomacula (arrowhead) also occur after ablation of *Pten* in adult mice. Scale bar, 20 μm.

B. Ultrastructural analysis of myelin pathology after adult inactivation of *Pten* with comma-shaped outfoldings (left panel), recurrent loops (middle panel) and tomacula (right panel). Scale bars, 1 μm.

protein translation and regulates cell size (Weichhart, 2012), but also plays a critical role in the formation of excessive myelin growth in the PNS, similar to its role in the CNS (Narayanan et al, 2009). These data also identify a possible target for the treatment of tomaculous neuropathies.

Implications for normal myelin growth

Judged from the earliest disease stages, the myelin pathology in *Pten* conditional mouse mutants appears to originate from small regions of non-compacted myelin membranes, *i.e.* paranodal loops and Schmidt–Lantermann incisures. The same sites contain high levels of phosphorylated AKT kinase. It is likely that this staining identifies a subcellular region of myelinating Schwann cells, in which PTEN is normally localized and antagonizes PI3 Kinase signalling, myelin growth and membrane turnover of the mature nerve. This function is required throughout life, as evidenced by similar myelin outfoldings and tomacula also in the nerves of adult mice, in which Cre recombination was induced by tamoxifen. Our findings are also in agreement with the model of PTEN as an inhibitor of myelination (Goebbels et al, 2010), which, in conjunction with the scaffolding protein Dlg1, serves as a break to prevent 'overmyelination' in the PNS (Cotter et al, 2010). We note that the carboxy-terminal PDZ ('postsynaptic density 95; discs large; zonula occludens 1′) binding motif of PTEN may not only interact with the stabilizing Dlg1 to regulate myelin formation. The PDZ binding motif of PTEN can also interact with PDZ domains of other resident scaffolding proteins that are present in Schwann cells, notably MAGI-2 and Par-3 (Feng et al, 2008; von Stein et al, 2005; Wu et al, 2000), both of which reside in non-compact myelin (Poliak et al, 2002). During normal Schwann cell development, Par3 is essential for establishing an intracellular polarity against the axon and thus for myelination (Chan et al, 2006). It is possible that at later stages Par3 recruits PTEN also to non-compact myelin where PtdIns(4,5)P2 and PtdIns(3,4,5)P3 levels have to be locally controlled. Also the periaxin gene encodes proteins with PDZ domains, L-periaxin and S-periaxin (Dytrych et al, 1998). These are expressed in Schwann cells and may play a role in the stabilization of the myelin sheath (Scherer et al, 1995). Given, that mutations of the human *PRX* gene and *Prx* null mutations in mice cause neuropathy with hypermyelination and focal myelin sheath thickening (Gillespie et al, 2000; Takashima et al, 2002), it is tempting to speculate that also the PDZ domain of periaxin may bind to and recruit PTEN.

A two-step model of myelin growth and pathology

Inhibiting mTORC1 with rapamycin in mice blocked pathological myelin outgrowth but had no obvious effect on wildtype Schwann cells. It is possible that the treatment effect, starting at age P13, when PNS myelination is already quite advanced, came simply too late to affect myelin formation in the wildtype. Alternatively, PTEN itself is the most rate-limiting regulator of developmental myelination, physically associated with membrane compartments that are thought to incorporate new membrane material (Özçelik et al, 2010). We propose that regions such as SLI and paranodal loops (in wildtype mice) are 'protected' by the presence of PTEN and only limited incorporation of newly synthesized myelin membranes takes place. This local PTEN 'brake' would function independently of regulated (mTORC1-dependent) cell growth and bulk membrane synthesis.

In contrast, in PTEN-deficient Schwann cells there is not only enhanced (mTORC1-dependent) synthesis of membranes, but also uncontrolled incorporation of these membranes into the myelin growth zones, constituting 'redundant' myelin. This may explain why blocking mTORC1 reduces the formation of tomacula and myelin outfoldings in PTEN mutants, but not myelination under physiological conditions. This model can also explain why the mere overexpression of constitutively active Akt (DDAkt) is by itself not efficient in inducing *de novo* myelination by Schwann cells or tomacula (Flores et al, 2008). The model is also in agreement with our finding that the number of myelin outfoldings (*i.e.* the 'primary' pathology) was less affected by rapamycin treatment than the number of tomacula found in sciatic nerve cross sections of Pten mutant mice. Here, we propose that the outfoldings as primary abnormalities are most likely caused by an altered (phosphoinositide-dependent) cytoskeletal rearrangement and altered membrane dynamics in mutant Schwann cells due to the loss of PTEN as the local 'brake', whereas the activation of AKT and mTORC1 in Schwann cells contributes to bulk membrane growth, and thus mostly to the size of focal myelin abnormalities resulting eventually in the formation of tomacula.

We note that for epithelial cells a heterogeneous and polarized lipid composition has been reported with PtdIns(3,4,5)P3 (along with its synthesizing enzyme PI3K) being enriched in the basolateral membrane (Gassama-Diagne et al, 2006). In contrast, PtdIns(4,5)P2 (along with PTEN) resides mostly in the apical domain (Martin-Belmonte et al, 2007). Epithelial cells and myelinating Schwann cell may be polarized in a similar way (Özçelik et al, 2010; Pereira et al, 2012), such that the outer abaxonal Schwann cell membrane containing PI3K and PtdIns(3,4,5)P3 represents the 'basolateral-like' domain, while the inner adaxonal domain and the Schmidt–Lanterman incisures are enriched in PtdIns(4,5)P2 and PTEN and represent an 'apical-like' domain. Interestingly, when PtdIns(3,4,5)P3 is ectopically inserted into the apical membrane of epithelial cells, these form membrane protrusions from the apical surface, which contain basolateral plasmamembrane proteins (Gassama-Diagne et al, 2006) and are enriched in filamentous actin. This is compatible with the idea that elevated PtdIns(3,4,5)P3 (in the absence of inhibitory PTEN) in the 'apical-like' Schwann cell compartment triggers pathological membrane deposition and myelin outfoldings.

Thus, we suggest a two-step model of myelin pathology for *Pten*-mutant mice: (i) abnormal PtdIns(3,4,5)P3 levels perturb the polarization of non-compact myelin membranes and cause focal, *e.g.* actin-dependent membrane protrusions, which is followed by (ii) enhanced AKT/mTORC1-signalling that contributes to uncontrolled membrane growth at these sites.

Why would elevated PtdIns(3,4,5)P3 in the 'apical-like' domain of a Schwann cell affect polarity, motility and membrane dynamics? Since actin nucleation is an important driving force of Schwann cell membrane movements (Fernandez-Valle et al, 1997) it is plausible that abnormally high PtdIns(3,4,5)P3 levels induce pathology by recruiting pleckstrin-homology (PH) domain containing regulatory proteins (such as GEFs and GAPs) as activators of small RhoGTPases and the actin cytoskeleton (Saarikangas et al, 2010). We note that GEFs, RhoGTPases and the downstream effector protein N-WASP (neural Wiskott–Aldrich syndrome protein) take part in normal myelin biogenesis (Benninger et al, 2007; Feltri et al, 2008; Nodari et al, 2007; Novak et al, 2011), and that loss of Frabin/FGD4 (a GEF protein with FYFE and PH domains) underlies demyelination in patients with CMT neuropathy type 4H (Stendel et al, 2007). We also note that the mTORC2 protein complex (which includes mTOR and Rictor) influences the dynamics of the actin cytoskeleton and is largely resistant to rapamycin (Weichhart, 2012).

Clinical implications

Tomacula, outfoldings and focal thickenings of the myelin sheath have been found in many peripheral neuropathies, including different forms CMT, HNPP, chronic inflammatory demyelinating neuropathy, paraproteinemic neuropathy, as well as in different animal models of peripheral nerve disorders (Sander et al, 2000). This suggests that a 'final common pathway' is precipitated by very different aetiologies, but how these tomacula are formed is not known. Abnormal phosphoinositide signalling emerges as a feature of severe neuropathies with focally pronounced myelin overgrowth, involving disease genes, such as in CMT4B1 (Mtmr2), CMT4B2 (Mtmr13) and CMT4H (Frabin/FGD4) that encode phosphoinositide binding FYFE and PH domains (Suter, 2007).

In conditional MTMR2 null mutant mice, the scaffolding protein Dlg1, which is by itself required for myelination (Bolis et al, 2009), has lost its normal abundance on the paranodal regions of Schwann cells (Bolino et al, 2004). Since PTEN is directly recruited by Dlg1 (Cotter et al, 2010), we hypothesize that a local secondary loss of PTEN could be part of the disease mechanism that underlies myelin outfoldings in CMT4B1 neuropathy.

Because phosphorylated AKT is an indicator of enhanced PI(3,4,5)P3 signalling, which underlies myelin outfoldings in *Pten* mutant mice, it could also be a molecular signature of other tomaculous neuropathies. However, little is known about the levels of pAKT in myelin (outfoldings) of these patients. Nevertheless, our data in mice suggest that AKT/mTORC1 signalling is important to drive the abnormal myelin growth. This identifies mTOR as a possible pharmacological target for therapy, independent of the steady-state level of pAKT and the rate of (pathological) myelin growth. Although systemic rapamycin would never be an option for the treatment of a peripheral neuropathy in man, the local (*e.g.* transdermal) administration of rapamycin analogs (Rauktys et al, 2008) can be explored for the treatment of specific aspects (*e.g.* neuropathic pain), using the available animal models.

MATERIALS AND METHODS

Mice

All experiments were performed according to the Lower Saxony State regulations for animal experimentation in Germany. *Pten*$^{flox/flox}$ and *PLP*-CreERT2 mice were genotyped as described (Leone et al, 2003;

The paper explained

PROBLEM:

Like the insulation of an electric cable, myelin membranes insulate nerve cell processes (axons), which allows the rapid propagation of nerve impulses. In the peripheral nervous system, these myelin membranes are made by Schwann cells. Genetic defects of peripheral myelination often block axon function and cause muscle weakness. A prominent neuropathological feature of several inherited neuropathies, including hereditary neuropathy with liability to pressure palsies (HNPP) and Charcot-Marie-Tooth disease type 4B1 (CMT4B1) are 'tomacula' or other forms of focally folded myelin. Despite major progress in defining the genetic cause of myelin diseases, the molecular mechanisms that result in abnormal myelin outgrowth in some forms of CMT, but not in others, have remained obscure.

RESULTS:

We have hypothesized that tomacula result from an uncontrolled local synthesis of myelin membranes, which is normally under control of specific growth factor receptors (neuregulin-1/ErbB2 as well as downstream PI3 Kinase and/or MAPK signalling). To test whether enhanced PI3K signalling [*i.e.* elevated phosphatidylinositol(3,4,5) trisphosphate levels activating the serine/threonine protein kinase AKT] would be sufficient to cause a tomaculous neuropathy, we generated mice, which lack PTEN (a lipid phosphatase antagonizing PI3K activity) selectively in Schwann cells. Indeed, this genetic modification was sufficient to cause focal hypermyelination, myelin outfoldings, and tomacula, even when induced in adult animals, *i.e.* after myelination is completed. This striking pathology is also dependent on active mTOR kinase, because the disease is significantly ameliorated in mice treated with the mTOR antagonist rapamycin.

IMPACT:

We suggest a model in which certain, non-compact regions of the myelin sheath are under lifelong 'protection' by PTEN, preventing abnormal membrane outgrowth. Furthermore, our data indicate that mTOR signalling is important to drive abnormal myelin growth, which identifies this serine/threonine protein kinase as a possible pharmacological target for the therapy of tomaculous neuropathies.

Lesche et al, 2002). *Cnp*-Cre mice were genotyped with primers Cnp-E3s, 5′-GCC TTC AAA CTG TCC ATC TC-3′ Cnp-E3as, 5′-CCC AGC CCT TTT ATT ACC AC-3′ and puro3, 5′-CAT AGC CTG AAG AAC GAG A-3′. Genomic DNA for PCR analysis was isolated from tail biopsies using Invisorb Spin Tissue Mini Kit (Invitek) according to the manufacturer's directions.

Rapamycin and tamoxifen treatment

Rapamycin (LC Laboratories) was dissolved in vehicle solution containing 5% polyethyleneglycol 400, 5% Tween 80 and 4% ethyl alcohol. Rapamycin or placebo (vehicle solution) was administered by intraperitoneal injections at 5 mg/kg for 5 days a week from postnatal day (P) 13–43. Tamoxifen (TM; Sigma) was dissolved in sunflower oil/ethanol (10:1) to a final concentration of 10 mg/ml. Two month-old mice received intraperitoneal injections at 100 μg TM per gram mouse weight once a day for 10 consecutive days and were analysed 3 months later. As carrier control sunflower oil/ethanol (10:1) was injected.

Protein analysis

Sciatic nerve lysates were homogenized in 1 ml of lysis-buffer (50 mM HEPES, pH 7.5, 150 mM NaCl, 1.5 mM MgCl2, 5 mM EGTA, 10% glycerol, 1% triton X-100, 2 mM Na3VO4) and protease inhibitors (Complete tablets, Roche, Basel, Switzerland) using an Ultraturrax (T8, Ika, Staufen, Germany) at highest settings (30–60 s). After incubation for 15 min on ice insoluble material was removed by centrifugation at 16.000 *g*, 4°C for 15 min. For Westernblot analysis, 40 μg of protein lysate was size-separated on 12% of SDS-polyacrylamide gels and blotted onto PVDF membranes (Hybond^{TM}-P, Amersham Biosciences, UK) by Bio-Rad western blotting method. Membranes were blocked in 5% milk powder (in PBS) for 1 h at room temperature. Primary antibodies directed against p-AKT (mRb, 1:1000; Cell Signaling), AKT (mRb, 1:1000; Cell Signaling), p-ERK (mRb, 1:1000; Cell Signaling); ERK (mRb, 1:1000; Cell Signaling), p-mTOR (mRb, 1:250; Cell Signaling), PTEN (mRb, 1:1000; Cell Signaling); p-S6 (mRb, 1:1000; Cell Signaling), and S6 (mRb, 1:1000; Cell Signaling) were diluted in blocking buffer and incubated overnight at 4°C. Membranes were washed 3 × 10 min in TBS-T buffer (50 mM Tris-HCl, pH 7.4, 150 mM NaCl and 0.05% Tween-20), followed by an incubation with horseradish peroxidase-conjugated secondary antibodies (1:5000, Jackson ImmunoResearch, West Grove, PA). After four more washes with TBS-T buffer, immunoreactive proteins were detected with an enhanced chemiluminescence kit (Western Lightning^{TM}, Westernblot Chemiluminescence Reagent Plus, PerkinElmer Life Sciences, Waltham, MA) according to the manufacturer's instructions.

Electron microscopy

For electron microscopy mice were anaesthetized with avertin (Sigma–Aldrich, St.Louis, MO) and perfused with 15 ml of Hanks balanced salt solution (HBSS, PAA laboratories, Pasching, Austria) followed by fixative (4% PFA + 0.1 M Phosphate buffer + 0.5% NaCl + 2.5% glutaraldehyde). Sciatic nerves were dissected at the level where the nerve exits the greater sciatic foramen. Nerves were contrasted with 1% osmium tetraoxide and embedded in epoxy resin. Semi-thin (0.5 μm) and ultra-thin (50–60 nm) sections were cut, using a microtome (RM 2155, Leica Microsystems, Wetzlar, Germany) with a diamond knife (Histo HI 4317, Diatome, Biel, Switzerland). Semithin sections were stained with azur-II-methylenblue for 1 min at 60°C. Light microscopic observation was performed using a Leica DM RXA microscope and a video frame grabber (ProgRes C14, Jenoptic, Jena, Germany). Images were digitalized with Openlab software

(Improvision, Coventry, UK). Ultra-thin sections were stained with 2% uranylacetate (30 min) and 1% lead citrate solution (12 min) and analysed using a LEO EM912AB electron microscope (Carl Zeiss NTS, Oberkochen, Germany). Pictures were taken with an on-axis 2048 × 2048 CCD camera (Proscan, Scheuring, Germany).

Histology and immunostaining

For immunohistochemistry mice were anaesthetized with Avertin and perfused with 15 ml of Hanks balanced salt solution, followed by 50 ml of 4% paraformaldehyde in PBS. Sciatic nerves were dissected and postfixed for 30 min at 4°C following embedding in paraffin and cutting in 5 μm slices (Microm HM400, Walldorf, Germany). Teased fibre preparations of sciatic nerves were performed immediately after perfusion and post fixation for 30 min on 4°C. The connective tissue was stripped off and nerves were separated into single fibres using a fine needle and a forceps and dried on an object slide. Slides containing paraffin sections or teased fibre preparations were incubated overnight with primary antibodies directed against MPZ (mM, 1:1000; provided by J. Archelos, University of Graz, Austria), p-AKT (pRb, 1:50; Cell Signaling), MAG (mM, 1:200; Chemicon), Dlg1 (pRb, 1:200; provided by A. Bolino, Dulbecco Telethon Institute, Milan, Italy) and Par-3 (pRb, 1:200; provided T. Pawson, Samuel Lunenfeld Research Institute, Toronto, Canada). After washing, slides were incubated with corresponding secondary Cy2 (1:100, Jackson ImmunoResearch) and Cy3 (1:1000, Jackson ImmunoResearch) conjugated antibodies for 1 h at room temperature. Sections were mounted with AquaPolymount (Polysciences, Warrington, PA). For analysis of myelin abnormalities, teased fibres were osmicated with 2% osmium tetraoxide for 5 h following dehydration in ethanol series. For depiction of Schmidt–Lanterman incisures postfixed sciatic nerves were osmicated and dehydrated in ethanol series before teasing. Slides were coverslipped with epoxy resin. Digital images were obtained by using a Zeiss Axiophot microscope, a Leica DM RXA microscope, and a LSM5 Zeiss confocal laser-scanning microscope. Image processing was performed with Openlab 2.2.3. (Improvision), Photoshop CS3 and Illustrator CS2 software (Adobe Systems, San Jose, CA).

Morphometry

Digitized, overlapping pictures (magnification 100×) of semithin sciatic nerve cross sections were fused to a continuous picture of a whole sciatic-nerve cross-section by using Photoshop CS (Adobe systems, San Jose, CA). Pictures were used to determine the numbers of myelinated axons, myelin abnormalities and g-ratios (100 randomly chosen fibres per nerve cross-section). G-ratios were determined by dividing the diameter of an axon by the diameter of the same axon including the myelin sheath. Fibres with myelin abnormalities in the plane of section were excluded. When not stated differently, measurements were performed from 3 age- and sex-matched mice per genotype and age. We implemented a plugin for the ImageJ software (http://rsb.info.nhi.gov/imagej, version 1.37), which allowed for semi-automated analysis of randomly selected sets of fibres. Plugin and source code are available online (http://gratio.efil.de).

Electrophysiology

Electrophysiology was performed on sciatic nerves of mice at 43 days of age. Mice were anaesthetized with Ketaminhydrochloride/Xylazinhydrochloride (100 mg/kg BW/8 mg/kg BW). A pair of steel needle electrodes (Schuler Medizintechnik, Freiburg, Germany) was placed subcutaneously along the nerve at sciatic notch (proximal stimulation). A second pair of electrodes was placed along the tibial nerve above the ankle (distal stimulation). Supramaximal square wave pulses lasting 100 ms were delivered using a Toennies Neuroscreen® (Jaeger, Hoechsberg, Germany). CMAP was recorded from the intrinsic foot muscles using steel electrodes. Both amplitudes and latencies of CMAP were determined. In addition, we measured the latency of late potentials resulting from the backfiring of antidromically activated motoneurons (F-waves). The distance between the two sites of stimulation was measured alongside the skin surface with fully extended legs and NCVs were calculated automatically from sciatic nerve latency measurements.

Statistical analaysis

Statistical analysis was performed by using two-tailed Student's *t*-test and the programs GraphPad Prism v4.03 (GraphPad, San Diego, CA, USA) and Microsoft Excel 2003. Results are expressed as means ± SEM.

Author contributions

SG, JHO and KAN developed study concept and design; JHO, SW, AP, GLW, and TR performed biochemical, histological and electronmicroscopical analyses under supervision of SG; TN performed electrophysiology on sciatic nerves under supervision of MWS; MG provided *Pten* flox mice; SG and KAN wrote the manuscript. All authors have read and approved the final manuscript.

Acknowledgements

We thank U. Bode for mouse genotyping. KAN and SG acknowledge grant support from the European Commission Seventh Framework Programme (FP7, NGIDD under grant agreement no. HEALTH-F2-2008-201535 and Leukotreat). This work was also supported by the BMBF (Leukonet) and the Myelin Project. KAN holds an ERC Advanced Grant (AxoGLIA).

The authors declare that they have no conflict of interest.

For more information

Heriditary Neuropathy with liability to preassure palsies (HNPP) web site:
http://www.hnpp.org

References

Adey NB, Huang L, Ormonde PA, Baumgard ML, Pero R, Byreddy DV, Tavtigian SV, Bartel PL (2000) Threonine phosphorylation of the MMAC1/PTEN PDZ binding domain both inhibits and stimulates PDZ binding. Cancer Res 60: 35-37

Adlkofer K, Frei R, Neuberg DH-H, Zielasek J, Toyka KV, Suter U (1997) Heterozygous peripheral myelin protein 22-deficient mice are affected by a progressive demyelinating tomaculous neuropathy. J Neurosci 17: 4662-4671

Benninger Y, Thurnherr T, Pereira JA, Krause S, Wu X, Chrostek-Grashoff A, Herzog D, Nave K.-A, Franklin RJM, Meijer D, *et al* (2007) Essential and

distinct roles for cdc42 and rac1 in the regulation of Schwann cell biology during peripheral nervous system development. J Cell Biol 177: 1051-1061

Berger P, Niemann A, Suter U (2006) Schwann cells and the pathogenesis of inherited motor and sensory neuropathies (Charcot-Marie-Tooth disease). Glia 54: 243-257

Bolino A, Muglia M, Conforti FL, LeGuern E, Salih MA, Georgiou DM, Christodoulou K, Hausmanowa-Petrusewicz I, Mandich P, Schenone A, *et al* (2000) Charcot-Marie-Tooth type 4B is caused by mutations in the gene encoding myotubularin-related protein-2. Nat Genet 25: 17-19

Bolino A, Bolis A, Previtali SC, Dina G, Bussini S, Dati G, Amadio S, Del Carro U, Mruk DD, Feltri ML, *et al* (2004) Disruption of Mtmr2 produces CMT4B1-like neuropathy with myelin outfolding and impaired spermatogenesis. J Cell Biol 167: 711-721

Bolis A, Coviello S, Bussini S, Dina G, Pardini C, Previtali SC, Malaguti M, Morana P, Del Carro U, Feltri ML, *et al* (2005) Loss of Mtmr2 phosphatase in Schwann cells but not in motor neurons causes Charcot-Marie-Tooth type 4B1 neuropathy with myelin outfoldings. J Neurosci 25: 8567-8577

Bolis A, Zordan P, Coviello S, Bolino A (2007) Myotubularin-related (MTMR) phospholipid phosphatase proteins in the peripheral nervous system. Mol Neurobiol 35: 308-316

Bolis A, Coviello S, Visigalli I, Taveggia C, Bachi A, Chishti AH, Hanada T, Quattrini A, Previtali SC, Biffi A, *et al* (2009) Dlg1, Sec8, and Mtmr2 regulate membrane homeostasis in Schwann cell myelination. J Neurosci 29: 8858-8870

Bonneick S, Boentert M, Berger P, Atanasoski S, Mantei N, Wessig C, Toyka KV, Young P, Suter U (2005) An animal model for Charcot-Marie-Tooth disease type 4B1. Hum Mol Genet 14: 3685-3695

Chan JR, Jolicoeur C, Yamauchi J, Elliott J, Fawcett JP, Ng BK, Cayouette M (2006) The polarity protein Par-3 directly interacts with p75NTR to regulate myelination. Science 314: 832-836

Chow CY, Zhang Y, Dowling JJ, Jin N, Adamska M, Shiga K, Szigeti K, Shy ME, Li J, Zhang X, *et al* (2007) Mutation of FIG4 causes neurodegeneration in the pale tremor mouse and patients with CMT4J. Nature 448: 68-72

Cotter L, Ozcelik M, Jacob C, Pereira JA, Locher V, Baumann R, Relvas JB, Suter U, Tricaud N (2010) Dlg1-PTEN interaction regulates myelin thickness to prevent damaging peripheral nerve overmyelination. Science 328: 1415-1418

Delague V, Jacquier A, Hamadouche T, Poitelon Y, Baudot C, Boccaccio I, Chouery E, Chaouch M, Kassouri N, Jabbour R, *et al* (2007) Mutations in FGD4 encoding the Rho GDP/GTP exchange factor FRABIN cause autosomal recessive Charcot-Marie-Tooth Type 4H. Am J Hum Genet 81: 1-16

Di Cristofano A, Pesce B, Cordon-Cardo C, Pandolfi PP (1998) Pten is essential for embryonic development and tumour suppression. Nat Genet 19: 348-355

Dytrych L, Sherman DL, Gillespie CS, Brophy PJ (1998) Two PDZ domain proteins encoded by the murine periaxin gene are the result of alternative intron retention and are differentially targeted in Schwann cells. J Biol Chem 273: 5794-5800

Fabrizi GM, Taioli F, Cavallaro T, Rigatelli F, Simonati A, Mariani G, Perrone P, Rizzuto N (2000) Focally folded myelin in Charcot-Marie-Tooth neuropathy type 1B with Ser49Leu in the myelin protein zero. Acta Neuropathol 100: 299-304

Fabrizi GM, Taioli F, Cavallaro T, Ferrari S, Bertolasi L, Casarotto M, Rizzuto N, Deconinck T, Timmerman V, De Jonghe P (2009) Further evidence that mutations in FGD4/frabin cause Charcot-Marie-Tooth disease type 4H. Neurology 72: 1160-1164

Feltri ML, Suter U, Relvas JB (2008) The function of RhoGTPases in axon ensheathment and myelination. Glia 56: 1508-1517

Feng W, Wu H, Chan LN, Zhang M (2008) Par-3-mediated junctional localization of the lipid phosphatase PTEN is required for cell polarity establishment. J Biol Chem 283: 23440-23449

Fernandez-Valle C, Gorman D, Gomez AM, Bunge MB (1997) Actin plays a role in both changes in cell shape and gene-expression associated with Schwann cell myelination. J Neurosci 17: 241-250

Flores AI, Narayanan SP, Morse EN, Shick HE, Yin X, Kidd G, Avila RL, Kirschner DA, Macklin WB (2008) Constitutively active Akt induces enhanced myelination in the CNS. J Neurosci 28: 7174-7183

Gassama-Diagne A, Yu W, ter Beest M, Martin-Belmonte F, Kierbel A, Engel J, Mostov K (2006) Phosphatidylinositol-3,4,5-trisphosphate regulates the formation of the basolateral plasma membrane in epithelial cells. Nat Cell Biol 8: 963-970

Genoud S, Lappe-Siefke C, Goebbels S, Radtke F, Aguet M, Scherer SS, Suter U, Nave K-A, Mantei N (2002) Notch1 control of oligodendrocyte differentiation in the spinal cord. J Cell Biol 158: 709-718

Gillespie CS, Sherman DL, Fleetwood-Walker SM, Cottrell DF, Tait S, Garry EM, Wallace VCJ, Ure J, Griffiths IR, Smith A (2000) Peripheral demyelination and neuropathic pain behavior in periaxin-deficient mice. Neuron 26: 523-531

Goebbels S, Oltrogge JH, Kemper R, Heilmann I, Bormuth I, Wolfer S, Wichert SP, Möbius W, Liu X, Lappe-Siefke C, *et al* (2010) Elevated phosphatidylinositol 3,4,5-trisphosphate in glia triggers cell-autonomous membrane wrapping and myelination. J Neurosci 30: 8953-8964

Hobert JA, Eng C (2009) PTEN hamartoma tumor syndrome: an overview. Genet Med 11: 687-694

Houlden H, King RHM, Wood NW, Thomas PK, Reilly MM (2001) Mutations in the 5′ region of the myotubularin-related protein 2 (MTMR2) gene in autosomal recessive hereditary neuropathy with focally folded myelin. Brain 124: 907-915

Lappe-Siefke C, Goebbels S, Gravel M, Nicksch E, Lee J, Braun PE, Griffiths IR, Nave K-A (2003) Disruption of Cnp1 uncouples oligodendroglial functions in axonal support and myelination. Nat Genet 33: 366-374

Leone DP, Genoud S, Atanasoski S, Grausenburger R, Berger P, Metzger D, Macklin WB, Chambon P, Suter U (2003) Tamoxifen-inducible glia-specific Cre mice for somatic mutagenesis in oligodendrocytes and Schwann cells. Mol Cell Neurosci 22: 430-440

Lesche R, Groszer M, Gao J, Wang Y, Messing A, Sun H, Liu X, Wu H (2002) Cre/loxP-mediated inactivation of the murine Pten tumor suppressor gene. Genesis 32: 148-149

Liang G, Cline GW, Macica CM (2007) IGF-1 stimulates de novo fatty acid biosynthesis by Schwann cells during myelination. Glia 55: 632-641

Martin-Belmonte F, Gassama A, Datta A, Yu W, Rescher U, Gerke V, Mostov K (2007) PTEN-mediated apical segregation of phosphoinositides controls epithelial morphogenesis through Cdc42. Cell 128: 383-397

Maurel P, Salzer JL (2000) Axonal regulation of Schwann cell proliferation and survival and the initial events of myelination requires PI 3-kinase activity. J Neurosci 20: 4635-4645

Meyer Zu Hörste G, Nave K-A (2006) Animal models of inherited neuropathies. Curr Opin Neurol 19: 464-473

Michailov GV, Sereda MW, Brinkmann BG, Fischer TM, Haug B, Birchmeier C, Role L, Lai C, Schwab MH, Nave K-A (2004) Axonal neuregulin-1 regulates myelin sheath thickness. Science 304: 700-703

Narayanan SP, Flores AI, Wang F, Macklin WB (2009) Akt signals through the mammalian target of rapamycin pathway to regulate CNS myelination. J Neurosci 29: 6860-6870

Nelis E, Erdem S, Tan E, Löfgren A, Ceuterick C, De Jonghe P, Van Broeckhoven C, Timmerman V, Topaloglu H (2002) A novel homozygous missense mutation in the myotubularin-related protein 2 gene associated with recessive Charcot-Marie-Tooth disease with irregularly folded myelin sheaths. Neuromuscul Disord 12: 869-873

Newbern J, Birchmeier C (2010) Nrg1/ErbB signaling networks in Schwann cell development and myelination. Semin Cell Dev Biol 21: 922-928

Newbern JM, Li X, Shoemaker SE, Zhou J, Zhong J, Wu Y, Bonder D, Hollenback S, Coppola G, Geschwind DH, *et al* (2011) Specific Functions for ERK/MAPK signaling during PNS development. Neuron 69: 91-105

Nodari A, Zambroni D, Quattrini A, Court FA, D'Urso A, Recchia A, Tybulewicz VLJ, Wrabetz L, Feltri ML (2007) Beta1 integrin activates Rac1 in Schwann cells to generate radial lamellae during axonal sorting and myelination. J Cell Biol 177: 1063-1075

Novak N, Bar V, Sabanay H, Frechter S, Jaegle M, Snapper SB, Meijer D, Peles E (2011) N-WASP is required for membrane wrapping and myelination by Schwann cells. J Cell Biol 192: 243-250

Ogata T, Iijima S, Hoshikawa S, Miura T, Yamamoto S-I, Oda H, Nakamura K, Tanaka S (2004) Opposing extracellular signal-regulated kinase and Akt pathways control Schwann cell myelination. J Neurosci 24: 6724-6732

Özçelik M, Cotter L, Jacob C, Pereira JA, Relvas JB, Suter U, Tricaud N (2010) Pals1 is a major regulator of the epithelial-like polarization and the extension of the myelin sheath in peripheral nerves. J Neurosci 30: 4120-4131

Pareyson D, Marchesi C, Salsano E (2009) Hereditary predominantly motor neuropathies. Curr Opin Neurol 22: 451-459

Pereira JA, Lebrun-Julien F, Suter U (2012) Molecular mechanisms regulating myelination in the peripheral nervous system. Trends Neurosci 35: 123-134

Poliak S, Matlis S, Ullmer C, Scherer SS, Peles E (2002) Distinct claudins and associated PDZ proteins form different autotypic tight junctions in myelinating Schwann cells. J Cell Biol 159: 361-372

Rauktys A, Lee N, Lee L, Dabora SL (2008) Topical rapamycin inhibits tuberous sclerosis tumor growth in a nude mouse model. BMC Dermatol 8: 1

Robinson FL, Niesman IR, Beiswenger KK, Dixon JE (2008) Loss of the inactive myotubularin-related phosphatase Mtmr13 leads to a Charcot–Marie–Tooth 4B2-like peripheral neuropathy in mice. Proc Natl Acad Sci USA 105: 4916-4921

Saarikangas J, Zhao H, Lappalainen P (2010) Regulation of the actin cytoskeleton-plasma membrane interplay by phosphoinositides. Physiol Rev 90: 259-289

Saitoh M, Pullen N, Brennan P, Cantrell D, Dennis PB, Thomas G (2002) Regulation of an activated S6 kinase 1 variant reveals a novel mammalian target of rapamycin phosphorylation site. J Biol Chem 277: 20104-20112

Sander S, Ouvrier RA, McLeod JG, Nicholson GA, Pollard JD (2000) Clinical syndromes associated with tomacula or myelin swellings in sural nerve biopsies. J Neurol Neurosurg Psychiatry 68: 483-488

Scherer SS, Wrabetz L (2008) Molecular mechanisms of inherited demyelinating neuropathies. Glia 56: 1578-1589

Scherer SS, Xu YT, Bannerman PG, Sherman DL, Brophy PJ (1995) Periaxin expression in myelinating Schwann cells: modulation by axon–glial interactions and polarized localization during development. Development 121: 4265-4273

Skre H (1974) Genetic and clinical aspects of Charcot-Marie-Tooth's disease. Clin Genet 6: 98-118

Stendel C, Roos A, Deconinck T, Pereira J, Castagner F, Niemann A, Kirschner J, Korinthenberg R, Ketelsen UP, Battaloglu E, *et al* (2007) Peripheral nerve demyelination caused by a mutant Rho GTPase guanine nucleotide exchange factor, frabin/FGD4. Am J Hum Genet 81: 158-164

Stiles B, Groszer M, Wang S, Jiao J, Wu H (2004) PTENless means more. Dev Biol 273: 175-184

Suter U (2007) Phosphoinositides and Charcot-Marie-Tooth disease: new keys to old questions. Cell Mol Life Sci 64: 3261-3265

Suzuki A, Nakano T, Mak TW, Sasaki T (2008) Portrait of PTEN: messages from mutant mice. Cancer Sci 99: 209-213

Takashima H, Boerkoel CF, De Jonghe P, Ceuterick C, Martin JJ, Voit T, Schröder JM, Williams A, Brophy PJ, Timmerman V, *et al* (2002) Periaxin mutations cause a broad spectrum of demyelinating neuropathies. Ann Neurol 51: 709-715

Taveggia C, Zanazzi G, Petrylak A, Yano H, Rosenbluth J, Einheber S, Xu X, Esper RM, Loeb JA, Shrager P, *et al* (2005) Neuregulin-1 type III determines the ensheathment fate of axons. Neuron 47: 681-694

Tersar K, Boentert M, Berger P, Bonneick S, Wessig C, Toyka KV, Young P, Suter U (2007) Mtmr13/Sbf2-deficient mice: an animal model for CMT4B2. Hum Mol Genet 16: 2991-3001

von Stein W, Ramrath A, Grimm A, Müller-Borg M, Wodarz A (2005) Direct association of Bazooka/PAR-3 with the lipid phosphatase PTEN reveals a link between the PAR/aPKC complex and phosphoinositide signaling. Development 132: 1675-1686

Waite KA, Eng C (2002) Protean PTEN: form and function. Am J Hum Genet 70: 829-844

Weichhart T (2012) Mammalian target of rapamycin: a signal kinase for every aspect of cellular life. Methods Mol Biol 821: 1-14

Wu X, Hepner K, Castelino-Prabhu S, Do D, Kaye MB, Yuan XJ, Wood J, Ross C, Sawyers CL, Whang YE (2000) Evidence for regulation of the PTEN tumor suppressor by a membrane-localized multi-PDZ domain containing scaffold protein MAGI-2. Proc Natl Acad Sci USA 97: 4233-4238

Zuchner S, Noureddine M, Kennerson M, Verhoeven K, Claeys K, Jonghe PD, Merory J, Oliveira SA, Speer MC, Stenger JE, *et al* (2005) Mutations in the pleckstrin homology domain of dynamin 2 cause dominant intermediate Charcot-Marie-Tooth disease. Nat Genet 37: 289-294

